This Page Is Inserted by IFW Operations
and is not a part of the Official Record

BEST AVAILABLE IMAGES

Defective images within this document are accurate representations of the original documents submitted by the applicant.

Defects in the images may include (but are not limited to):

- BLACK BORDERS
- TEXT CUT OFF AT TOP, BOTTOM OR SIDES
- FADED TEXT
- ILLEGIBLE TEXT
- SKEWED/SLANTED IMAGES
- COLORED PHOTOS
- BLACK OR VERY BLACK AND WHITE DARK PHOTOS
- GRAY SCALE DOCUMENTS

IMAGES ARE BEST AVAILABLE COPY.

**As rescanning documents *will not* correct images,
please do not report the images to the
Image Problem Mailbox.**

Document AS11
Appl. No. 10/685,801

JOURNAL OF VIROLOGY, Nov. 1997, p. 8808–8820
0022-538X/97/$04.00+0
Copyright © 1997, American Society for Microbiology
Vol. 71, No. 11

Structure-Based Identification of an Inducer of the Low-pH Conformational Change in the Influenza Virus Hemagglutinin: Irreversible Inhibition of Infectivity

LUCAS R. HOFFMAN,[1] I. D. KUNTZ,[1,2] AND JUDITH M. WHITE[3]*

Department of Biochemistry and Biophysics, University of California, San Francisco, San Francisco, California 94143-0448,[1] and Department of Pharmaceutical Chemistry, University of California, San Francisco, San Francisco, California 94143-0446,[2] and Department of Cell Biology, University of Virginia, Charlottesville, Virginia 22908[3]

Received 13 March 1997/Accepted 29 July 1997

Past efforts to employ a structure-based approach to design an inhibitor of the fusion-inducing conformational change in the influenza virus hemagglutinin (HA) yielded a family of small benzoquinones and hydroquinones. The most potent of these, *tert*-butyl hydroquinone (TBHQ), inhibits both the conformational change in HA from strain X:31 influenza virus and viral infectivity in tissue culture cells with 50% inhibitory concentrations in the micromolar range (D. L. Bodian, R. B. Yamasaki, R. L. Buswell, J. F. Stearns, J. M. White, and I. D. Kuntz, Biochemistry 32:2967–2978, 1993). A new structure-based inhibitor design search was begun which involved (i) the recently refined crystal structure (2.1-Å resolution) of the HA ectodomain, (ii) new insights into the conformational change, and (iii) improvements in the molecular docking program, DOCK. As a result, we identified new inhibitors of HA-mediated membrane fusion. Like TBHQ, most of these molecules inhibit the conformational change. One of the new compounds, however, facilitates rather than inhibits the HA conformational change. Nonetheless, the facilitator, diiodofluorescein, inhibits HA-mediated membrane fusion and, irreversibly, infectivity. We further characterized the effects of inhibitors from both searches on the conformational change and membrane fusion activity of HA as well as on viral infectivity. We also isolated and characterized several mutants resistant to each class of inhibitor. The implications of our results for HA-mediated membrane fusion, anti-influenza virus therapy, and structure-based inhibitor design are discussed.

All enveloped viruses penetrate host cells by means of a membrane fusion event between the virus and a host cell membrane (20). The orthomyxovirus influenza virus enters cells by receptor-mediated endocytosis. Upon delivery to endosomes, the low pH therein triggers an irreversible conformational change in the viral transmembrane protein hemagglutinin (HA). This conversion, in turn, induces fusion of the viral and endocytic membranes, thus allowing the viral genetic material to enter the cell to initiate an infection. HA exists on the surface of the virus as a trimer, and each monomer consists of two chains, HA1 and HA2. In terms of virus entry, the HA1 subunit is responsible for binding the virus to host cell sialic acid-containing receptors, whereas the HA2 subunit, which houses the fusion peptide, is responsible for fusion (53).

When influenza virus is treated with the protease bromelain, a soluble trimeric HA ectodomain, known as BHA, is released. The X-ray crystal structure of the neutral-pH form of BHA has been solved to a 2.1-Å resolution (44, 54). In this structure, the fusion peptides are inserted into the center of the trimer; they are largely inaccessible to solvent and approximately 100 Å away from the sialic acid binding sites and hence the target membrane (54). Recently, the structure of a proteolyzed form of low-pH-treated BHA, known as TBHA2, was solved by X-ray diffraction analysis (7). This structure reveals four major changes in BHA at low pH. First, the globular heads comprised by HA1 have become susceptible to trypsinization and have been removed. Second, residues 54 to 76 of HA2 (HA2 54–76) which were unstructured in neutral-pH BHA, are helical in TBHA2. Third, residues 106 to 112 of HA2 (HA2 106–112 region) have undergone a helix-to-loop transition at low pH. Fourth, the C-terminal ~20 residues of the HA2 ectodomain have become disordered. Although recent structural (49) and biochemical (45) data indicate that TBHA2 is likely representative of a postfusion conformation of HA, the low-pH transitions evidenced by the structure are almost certainly important in forming the active fusogenic form. For example, separation of the globular head domains is a necessary antecedent of fusion peptide exposure (18, 24), the helix-to-loop transition of HA2 106–112 removes hydrogen bonds and salt bridge interactions that tether the fusion peptides (7, 11), and the loop-to-helix transition of HA2 54–76 apparently transports the fusion peptides towards the target membrane to initiate fusion (7, 30a).

Since the HA conformational change is absolutely required for infection and occurs early in the viral life cycle, this event is an attractive target for pharmacologic intervention. We previously described an approach for identifying inhibitors of the HA conformational change (6) employing the 3-Å-resolution structure of BHA in conjunction with a computer-searching algorithm known as DOCK (12, 33). Given the three-dimensional coordinates of a target macromolecule, DOCK characterizes the molecular surface chemically and geometrically and then scans a database for small molecules predicted to interact with a user-defined target site on the macromolecular surface. Our original search for HA inhibitors focused on the region surrounding the fusion peptide. We applied DOCK to a pocket on HA that is formed partially by residues of the fusion peptide with the expectation that a molecule that binds to the site would stabilize the region in its prefusion conformation. From the compounds suggested by DOCK, we identified a family of related benzoquinones and hydroquinones that inhibit the acid-induced conformational change of BHA in vitro as well as viral infectivity in cell culture at micromolar concentrations. The most potent of these inhibitors is *tert*-butyl hydroquinone (TBHQ), a small molecule that inhibits both the conformational change and viral infectivity in the range of 5 to 10 μM (5, 6).

---

* Corresponding author. Mailing address: Department of Cell Biology, University of Virginia, Charlottesville, VA 22908. Phone: (804) 924-2593. Fax: (804) 982-3912. E-mail: jw7g@virginia.edu.

Three major advances have been made since the identification of TBHQ as an inhibitor of the low-pH-induced conformational change in HA that augured well for a new round of inhibitor design: the resolution of the BHA crystal structure has increased, the DOCK program has been refined, and fresh insights have been provided into the mechanism of the conformational change in HA. The availability of structural data about BHA to a 2.1-Å resolution (44) offered more information concerning potential target sites. DOCK itself was improved, having gained a more chemically descriptive scoring function for ranking potential inhibitors (30). Furthermore, the database of compounds available for searching grew approximately threefold (Molecular Design Ltd., San Leandro, Calif.). The most recent version of DOCK employs a rigid-body minimization step designed to allow a more exhaustive search of possible ligand binding orientations (19). As described above, recent advances in the understanding of the HA conformational change have also been made, including the crystallographic identification of the final low-pH conformation of BHA (7) and evidence of the importance of regions distal to the fusion peptide in achieving the fusion-active conformation (8, 18, 24, 30a, 49). We therefore initiated a new round of structure-based inhibitor searching by targeting two sites surrounding HA2 54–81, the region of HA2 that undergoes the so-called "spring-loaded" loop-to-helix transition at low pH.

(Portions of this work were presented at the Third International Conference on Options for the Control of Influenza, Cairns Australia, 4 to 9 May 1996.)

MATERIALS AND METHODS

Cells and viruses. Clone 2 Madin-Darby canine kidney cells (MDCK2) and the HA-expressing cell line HA300a^{++} were cultivated as described previously (6, 25). X:31 influenza virus (clone C-22) was grown as described previously (6).

Viruses resistant to TBHQ were isolated by two procedures. In the first procedure, allantoic fluid from eggs infected with plaque-purified virus was used to infect MDCK2 monolayers at a multiplicity of infection (MOI) of 0.01 PFU/cell. Allantoic fluid was diluted in minimal essential medium with Earle's basic salts (MEM-EBSS) containing 25 mM HEPES, penicillin-streptomycin, and 1% fetal bovine serum (FBS) (hereafter referred to as diluent). TBHQ (100 or 10 μM) was added, and the mixture was adsorbed to cells for 1 h at 37°C. The medium was then replaced with primary overlay medium (2× MEM-EBSS with 2× penicillin-streptomycin, 50 mM HEPES, and 5% FBS mixed with an equal volume of 1% SeaPlaque agarose). Trypsin was added to a final concentration of 10 μg/ml, and the overlay was allowed to harden at room temperature. The cells were then returned to a 37°C, 5% CO_2 incubator. The infection was allowed to proceed for 36 h, at which time 2.5 ml of a second overlay medium (equal volumes of 2× MEM-EBSS with 2× penicillin-streptomycin, 50 mM HEPES, 5% FBS, and 1.8% SeaPlaque agarose, also containing 0.003% neutral red solution [Sigma]) was allowed to harden over the first overlay, and the cells were returned to the incubator for an additional 4 h. Plaques containing virus were harvested with sterile 200-μl pipette tips and resuspended in 2 ml of diluent for further passaging. This process was repeated eight times, with the exception that in passages 2 to 8, inhibitor was added to the primary overlay. TBHQ-resistant virus was then amplified by one passage on MDCK2 cells in virus-free, TBHQ-free diluent lacking trypsin. After 48 h of infection, the diluent-containing virus was harvested and cleared of cellular debris. The resultant virus stock was then tested for sensitivity to TBHQ by both plaque assay and enzyme-linked immunosorbent assay (ELISA) and prepared for sequencing as described below.

In the second procedure, the initial infection was carried out as described above, but with an MOI of 1 PFU/cell and in the presence of 3 mM TBHQ, a concentration that is nontoxic to MDCK2 cells as assessed by trypan blue exclusion assay (1). After 1 h of adsorption, the diluent containing virus and inhibitor was removed and replaced with liquid diluent overlay containing 100 μM TBHQ. After 48 h of incubation at 37°C with 5% CO_2, the overlay containing virus was harvested. This stock was then used to isolate TBHQ-resistant viruses through one round of plaque purification in the presence of 100 μM TBHQ. The resultant TBHQ-resistant isolates were then amplified and processed as described above.

Viruses resistant to diiodofluorescein (C22) were isolated as described above by the single-round, high-MOI procedure in the presence of 1 mM C22, a concentration that is nontoxic to MDCK2 cells as determined by both trypan blue exclusion and [^{35}S]methionine incorporation (1).

Inhibitors. TBHQ and C22 were purchased from Aldrich. Phenolphthalein monophosphate disodium (S22), zincon-Na (S23), eosin B (C13), bromopyrogallol red (S15), eosin (S17), 3′-dephospho-coenzyme A (C26), and stilbazo (C29) were purchased from Sigma. Maybridge NRB00384 (S19), NRB08312 (S110), NRB02903 (C19), and DFP0028 (S28) were purchased from Maybridge via Ryan Scientific.

Infectivity assays. Plaque assays of MDCK2 cells were carried out as described previously (41) with the following modifications. Virus released from MDCK2 cells (which express the inactive precursor form of HA, HA0) was pretreated with 10 μg of trypsin per ml for 30 min at room temperature; trypsin was quenched by dilution of virus into diluent (which contains 1% FBS). Monolayers of MDCK2 cells in six-well plates were washed twice with phosphate-buffered saline (PBS) and inoculated with 0.25 ml of virus in diluent for 1 h at 37°C, with rocking every 15 min. At this time, 2.5 ml of primary overlay medium containing 10 μg of trypsin per ml was added. After the overlay was allowed to harden at room temperature, the cells were returned to a 37°C, 5% CO_2 incubator for 36 h. At this time, 2.5 ml of the second overlay medium containing 0.003% neutral red was added and allowed to harden, and the cells were returned to the incubator. Plaques were counted 6 h later. For the single-cycle infection assay, virus was adsorbed to cells for 1 h at 4°C. The medium was then removed and replaced with fresh, prewarmed diluent. The cells were then returned to the 37°C, 5% CO_2 incubator. After 15 h, the medium was removed, treated with 10 μg of trypsin per ml for 30 min at room temperature, and assayed for virus concentration by plaque assay. ELISAs for single-cycle growth and MTT (3-[4,5-dimethylthiazol-2-yl]-2,5-diphenyltetrazolium bromide) cell viability assays were carried out as described previously (6).

Hemolysis assay. The pH at which the different viruses lyse fresh, human type A$^+$ erythrocytes was determined as described previously (11) with the following modifications. Incubations at low pH were conducted for 15 min at 37°C, and hemoglobin was detected spectrophotometrically at 550 nm. Inhibition of hemolysis as a function of pH was performed and calculated as described previously (6).

Virus genome sequencing. Virus isolates harvested in liquid media were pelleted, and their RNA genomes were purified as described previously (57). The HA genes were then reverse transcribed with a primer corresponding to coding strand nucleotides 15 to 35, numbered according to the cDNA sequence of X:31 HA given in GenBank (accession no. J02090) by the method of Xu et al. (57). The cDNAs were then amplified by PCR with one primer corresponding to coding strand nucleotides 36 to 56 and another complementary to coding strand nucleotides 1693 to 1712 in the noncoding direction. The products of this amplification were then sequenced with the *fmol* cycle sequencing kit (Promega). The 10 primers used for sequencing mutant and wild-type HA genes correspond to coding strand nucleotides 36 to 56, 282 to 306, 454 to 477, 677 to 700, 857 to 881, 1025 to 1048, 1191 to 1214, 1350 to 1373, 1497 to 1520, and 1596 to 1640.

Preparation and purification of biotinylated BHA. Purified X:31 virus was biotinylated, and its HA was released with bromelain as described for HA-expressing cells (24) with the following modifications. Thirteen milligrams of virus was suspended in 3 ml of ice-cold PBS containing 1 mg of NHS-LC-biotin (Amersham) per ml and incubated at 4°C for 45 min. The virus was then pelleted by centrifugation in a TLA100.3 rotor at 55,000 rpm for 30 min at 4°C. The supernatant was aspirated, and the virus pellet was resuspended in 50 mM glycine in ice-cold PBS. The virus was pelleted as before and resuspended in 1 ml of 0.1 M Tris-HCl (pH 8). Bromelain was added to give a final concentration of 2.5 mg/ml. Concentrated β-mercaptoethanol (7.7 μl) was added, and the mixture was incubated at 37°C overnight. The virus was then pelleted as described above. Biotinylated BHA was then purified from the supernatant on a column of ricin-I agarose (Sigma). The column was washed with MES (morpholineethanesulfonic acid)-saline-succinate-HEPES buffer (MSSH; 10 mM HEPES, 10 mM MES, 10 mM succinate, 0.10 M NaCl [pH 7.0]), and the bound BHA was eluted with 0.2 M galactose in MSSH. Biotinylated BHA was detected after sodium dodecyl sulfate-polyacrylamide gel electrophoresis (SDS-PAGE) on 12% polyacrylamide gels, with transfer of proteins to Immobilon-P membranes (Millipore) and blotting with streptavidin-conjugated horseradish peroxidase (HRP) (24).

Protease assays for the HA conformational change: thermolysin digestion. Thermolysin has been shown to digest exposed fusion peptides in the final low-pH conformation of BHA (7, 10). To assay for this conformational change, 100-μl aliquots of purified, biotinylated BHA (1 μg/ml in MSSH) were adjusted to the indicated pH value by the addition of 1 M acetic acid for the indicated time and then reneutralized with 1 M NaOH. Equivalent amounts of MSSH buffer were added to pH 7 controls. $CaCl_2$ and thermolysin (Sigma) were added to final concentrations of 1 mM and 10 μg/ml, respectively. The mixture was incubated at 37°C for 2 h, and the reaction was then quenched with EDTA (10 mM final concentration). Samples were then processed for SDS-PAGE, transferred to Immobilon-P membranes, and probed with streptavidin-HRP as described in

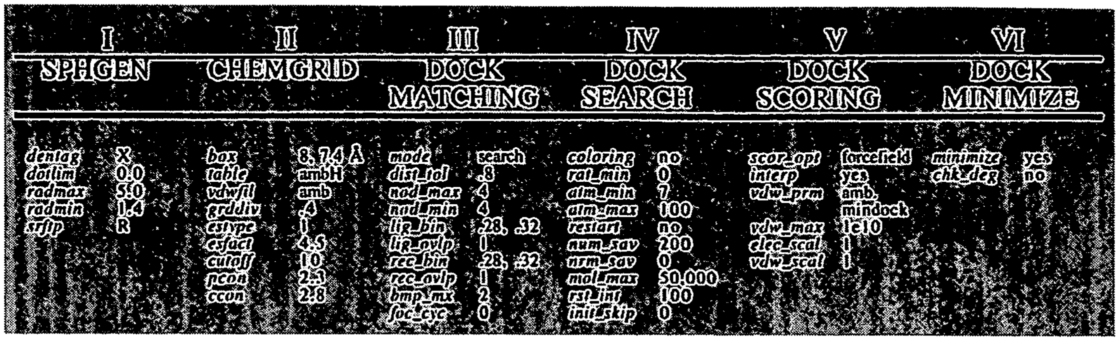

I SPHGEN		II CHEMGRID		III DOCK MATCHING		IV DOCK SEARCH		V DOCK SCORING		VI DOCK MINIMIZE	
dentag	X	*box*	8, 7.4 Å	*mode*	search	*coloring*	no	*scor_opt*	forcefield	*minimize*	yes
dotlim	0.0	*table*	ambH	*dist_tol*	.8	*rat_min*	0	*interp*	yes	*chk_deg*	no
radmax	5.0	*vdwfil*	amb	*nod_max*	4	*atm_min*	7	*vdw_prm*	amb.		
radmin	1.4	*grddiv*	.4	*nod_min*	4	*atm_max*	100		mindock		
srfip	R	*estype*	1	*lig_bin*	.28, .32	*restart*	no	*vdw_max*	1e10		
		esfact	4.5	*lig_ovlp*	1	*num_sav*	200	*elec_scal*	1		
		cutoff	10	*rec_bin*	.28, .32	*nrm_sav*	0	*vdw_scal*	1		
		pcon	2.3	*rec_ovlp*	1	*mol_max*	50,000				
		ccon	2.8	*bmp_mx*	2	*rst_int*	100				
				foc_cyc	0	*init_skip*	0				

FIG. 1. Input parameters for the computer programs SPHGEN, CHEMGRID, and DOCK3.5. The variables abbreviated above are defined in the DOCK3.5 user's manual.

reference 24 and above. Films of each gel were analyzed by densitometry. Four standards, containing 100, 60, 20, and 10% of the input biotinylated BHA used in each analysis, were loaded on each gel and used to generate a standard curve of the percent protein versus the HA2 signal.

Proteinase K assay. Low-pH-treated BHA was digested by proteinase K (51). To assay for this conformational change, biotinylated BHA was treated at low pH and reneutralized as described above and then incubated with proteinase K (5,000:1 [wt/wt] BHA-proteinase K) for 30 min at 37°C. Samples were then processed for SDS-PAGE and streptavidin-HRP blotting as described above. Digestion of the HA1 band was used as a qualitative measure of the conformational change.

Fusion assays. Fresh, type A^+ human erythrocytes (RBCs) were lysed by hypotonic shock and resealed in the presence of either ethidium bromide or β-galactosidase as described previously (14, 29). RBCs were then washed and adsorbed onto monolayers of HA300a^{++} cells. Prior to RBC addition, HA300a^{++} cells were treated with either neuraminidase (28) or a mixture of neuraminidase and trypsin (to cleave HA0 to HA1 and HA2 (29). After being washed to remove unbound RBCs, the RBC-cell complexes were exposed to either pH 4.9 or 7 buffer as described previously (29), reneutralized, and processed for microscopy. For the ethidium bromide assay, cells were visualized in a fluorescent microscope to detect transfer of ethidium bromide to the HA300a^{++} cells (29). For the β-galactosidase assay, RBC-cell complexes were treated with 20 mg of neuraminidase per ml (with shaking) to remove bound but unfused RBCs. The cells were then fixed in 0.05% glutaraldehyde in PBS for 10 min at room temperature and processed for the detection of β-galactosidase activity as described previously (1).

DOCK. DOCK3.5 (19) was employed as described in Results with crystallographic coordinates for BHA at a 2.1-Å resolution (44) and user-defined variables as listed in Fig. 1. Spheres for each site description were selected interactively from the SPHGEN output. Approximately 150,000 molecules were screened for their predicted affinities for each of the two sites analyzed with a rigid-body minimization step and an AMBER-based potential function for evaluating predicted interactions (19, 30). The top-scoring 200 molecules from the search to each site were screened with computer graphics (15). Graphical screening involved evaluation of contacts with charged versus hydrophobic regions of the sites and well- versus poorly conserved regions of the sites. The predicted solubility of the compounds was also considered. By these criteria and based on commercial availability, 25 molecules per site were selected from the original 200 for in vitro screening.

Computer modeling of HA. HA drawings were produced with the MidasPlus software system from the Computer Graphics Laboratory, University of California, San Francisco (15). Coordinates of HA used for figures are from entry 5HMG (46) in the Brookhaven protein data bank (3).

RESULTS

Identification of new sites and test compounds. The region of HA chosen for the new structure-based inhibitor search contains the interfaces between the globular heads (an intermonomer interface) and those between HA1 and HA2 (intramonomer interface) (Fig. 2) (44, 54). Two neighboring sites were defined, referred to as 2A and 2B, and were used for independent searches (Fig. 2). Site 1A, the pocket used in the original search that identified TBHQ (6), is also shown. Note that there are three copies of each site per trimer. The limits of the pockets of both sites 2A and 2B are partially defined by residues from HA2 54–81, the region of HA that undergoes a random coil-to-coiled-coil transition at low pH (7, 8). Both sites exhibit many intermonomer and intramonomer interactions, involving both hydrophobic and polar contacts. Any of these interactions are potential targets for stabilization or destabilization by a small molecule. The sites were also chosen for their sizes, their concave shapes, and their high level of sequence conservation. For both sites, surface residues are 98% identical among all influenza viruses of the H3 subtype and 78% identical among all influenza A viruses (data compiled from appendix B in reference 5).

Figure 1 lists the parameters used in the new DOCK search. Twenty-five molecules per site were selected for in vitro screening as described in Materials and Methods. Twelve of these compounds have been tested to date; their structures are diagrammed in Fig. 3.

Testing of compounds. We previously showed, using a scintillation proximity assay, that TBHQ inhibits the fusion-inducing conformational change in the influenza virus HA with a 50% inhibitory concentration (IC_{50}) of 5 μM. As a starting point for our study, we have developed a new quantitative assay for the HA conformational change and have used it to assess the effects of TBHQ. The assay employs purified, biotinylated BHA and relies on the observation that following treatment at low pH, the exposed fusion peptide is sensitive to thermolysin digestion, resulting in a decrease in apparent molecular mass of HA2 from approximately 20 kDa to 18 kDa (10, 35). As seen in Fig. 4A, when low-pH-treated BHA is treated with thermolysin, the HA2 band is digested, and a band of approximately 18 kDa labeled HA2* appears (lane 2 [also see lane 6]). However, if TBHQ is included during the low-pH treatment, the HA2 band is largely protected (compare lane 4 with lane 2). If TBHQ is added after the low-pH treatment (post control), the HA2 band is not protected (lane 6). To quantitate the extent of protection, we analyzed the intensity of the HA2 band (see Materials and Methods for details). This method proved to be a more reproducible measure of the extent of protection than quantitation of the relatively faint HA2* band. The HA2* band is likely faint because of loss of biotinylated residues (relative to HA2) and because, using our protocol (for comparison, see reference 10 in which BHA is treated with trypsin before digestion with thermolysin), the HA2* band is not stable, but becomes further digested by thermolysin. By this method of quantitation, the amount of TBHQ required to inhibit the conformational change displayed an IC_{50} of ~12 μM (Fig. 3B), in reasonable agreement with our prior results (6).

We next tested 12 of the new compounds selected by DOCK (Fig. 3) for their effects on the low-pH conformational change in HA by using the thermolysin assay. Compounds that had an effect in the thermolysin assay were further tested for their ability to inhibit virus infectivity in tissue culture and for cellular toxicity. The compiled data are shown in Table 1. Figure 4C displays the sensitivity of BHA to thermolysin in the presence of two of the inhibitors identified. As seen in Fig. 4C and Table 1, phenolphthalein monophosphate (S22) inhibits the conformational change of BHA (IC_{50} of <100 μM) and viral infectivity (IC_{50} of 40 μM [Table 1]). Thus, S22, although less potent, behaves quite similarly to our previously identified inhibitor, TBHQ. S19 also inhibits the conformational change, but its potency in the infectivity assay was much higher than in the conformational change assay (Table 1). In contrast to these inhibitors, and as seen in Fig. 4C and D and 5C and D, C22 facilitates the conformational change (50% effective concentration of approximately 8 μM) yet inhibits viral infectivity (IC_{50} of 8 μM [Table 1]). C22 thus defines a new class of agents that appear to inhibit viral infectivity by potentiating the HA

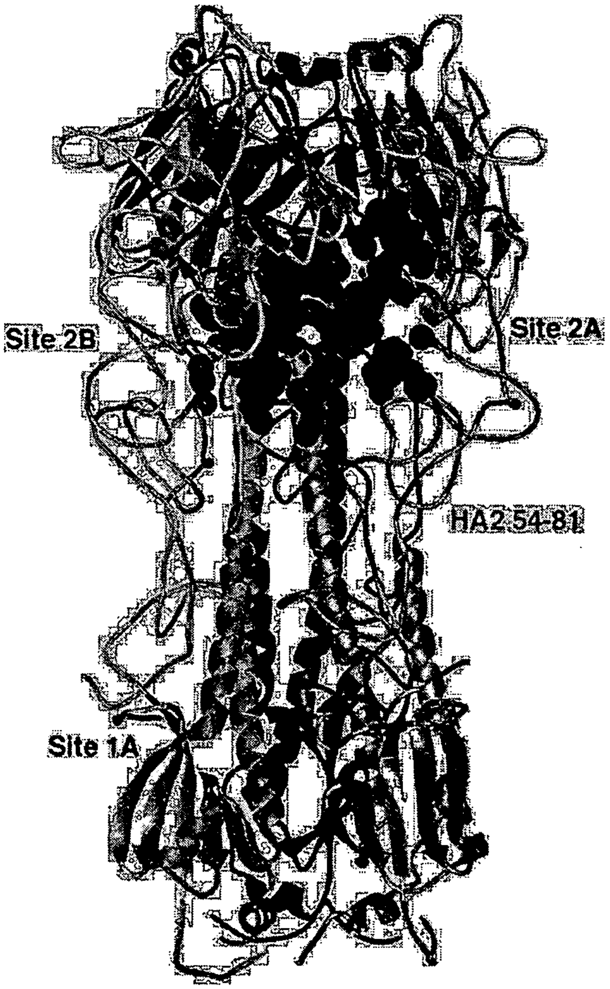

FIG. 2. Locations of new DOCK sites in the neutral-pH structure of BHA. The coordinates used are from the Brookhaven protein data bank, entry 5HMG. Monomers in the BHA trimer are colored gray, yellow, and green. Dots indicate locations of spheres used in orienting potential ligands computationally for evaluation of predicted interaction with a site. Blue dots, site 2A; red dots, site 2B; magenta, HA2 54-81: black area, site 1A (6).

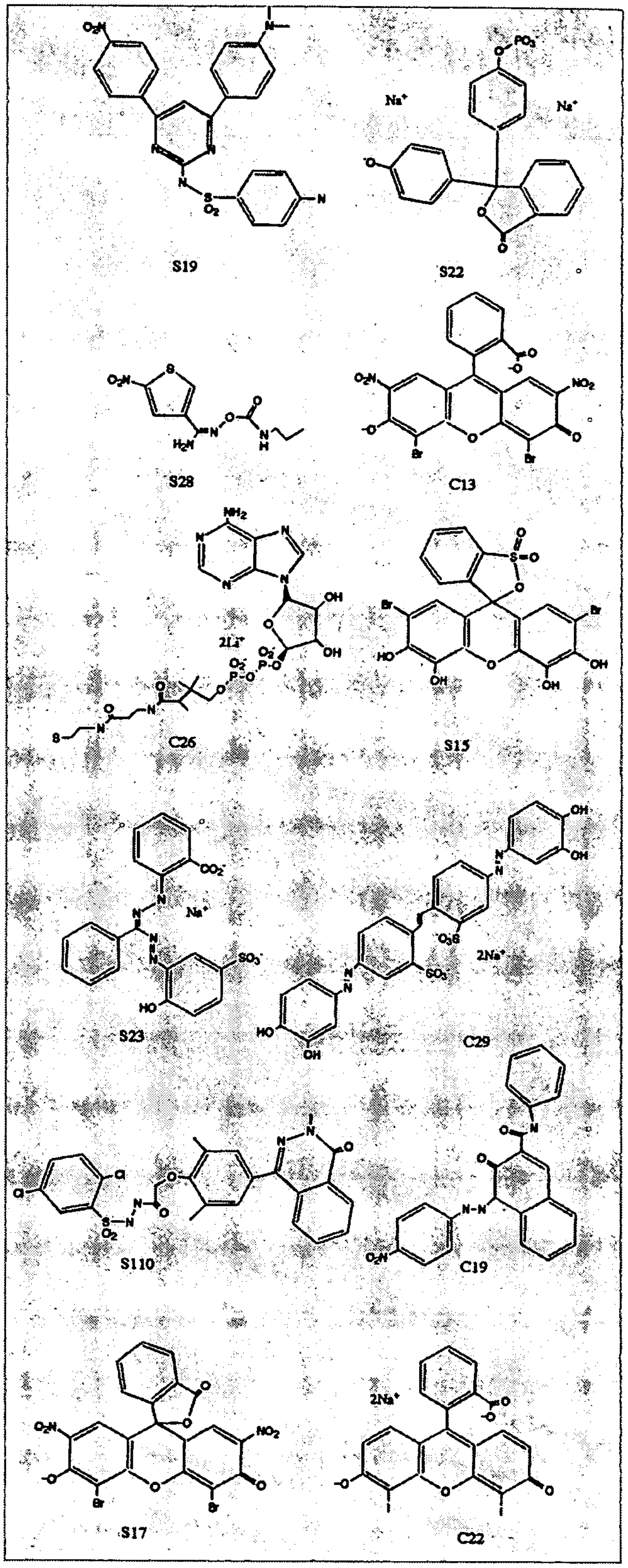

FIG. 3. Structures of compounds selected by DOCK as potential HA inhibitors. The C or S prefix indicates whether the compound came from DOCK output to site 2A or 2B, respectively.

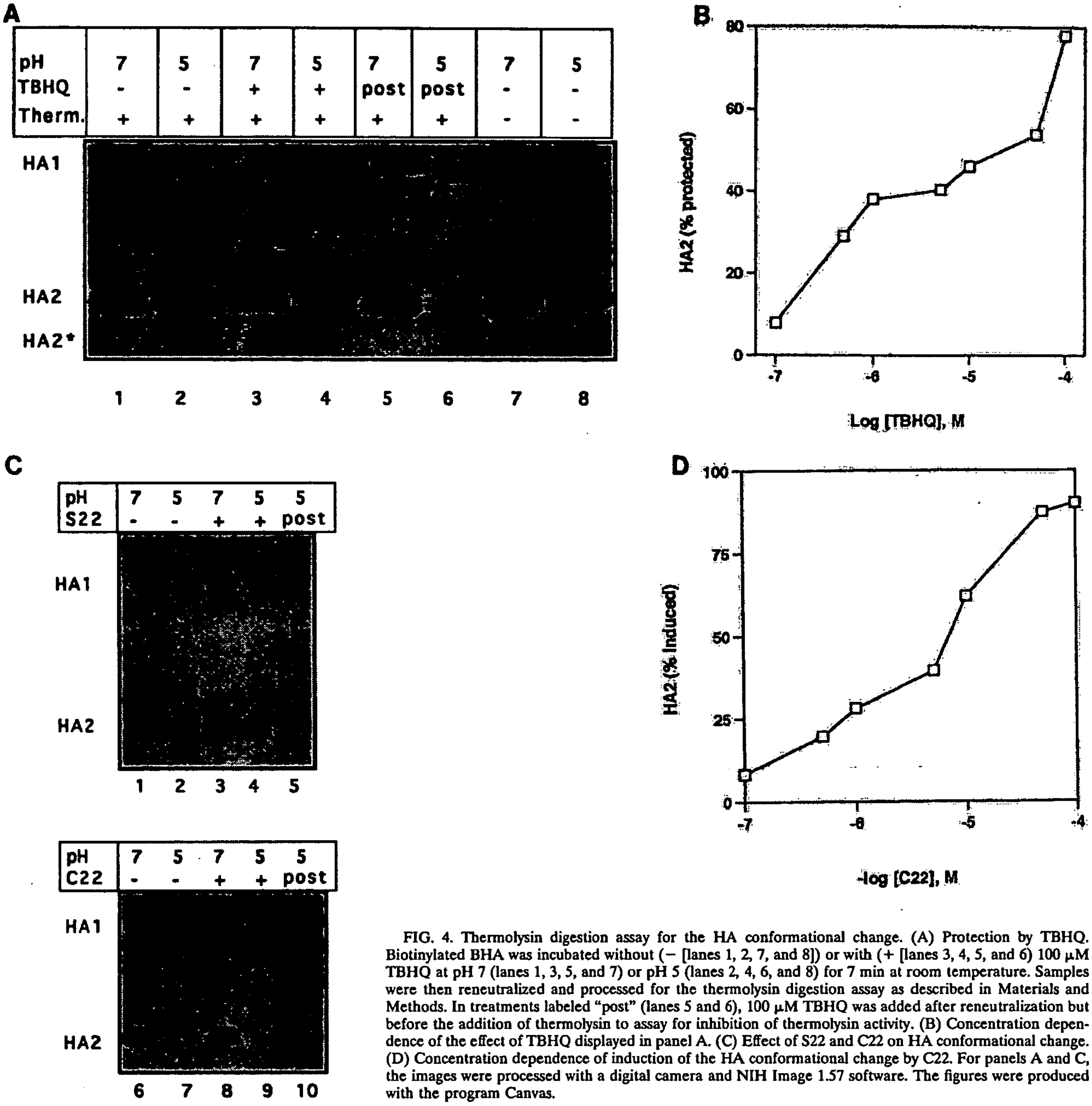

FIG. 4. Thermolysin digestion assay for the HA conformational change. (A) Protection by TBHQ. Biotinylated BHA was incubated without (− [lanes 1, 2, 7, and 8]) or with (+ [lanes 3, 4, 5, and 6]) 100 μM TBHQ at pH 7 (lanes 1, 3, 5, and 7) or pH 5 (lanes 2, 4, 6, and 8) for 7 min at room temperature. Samples were then reneutralized and processed for the thermolysin digestion assay as described in Materials and Methods. In treatments labeled "post" (lanes 5 and 6), 100 μM TBHQ was added after reneutralization but before the addition of thermolysin to assay for inhibition of thermolysin activity. (B) Concentration dependence of the effect of TBHQ displayed in panel A. (C) Effect of S22 and C22 on HA conformational change. (D) Concentration dependence of induction of the HA conformational change by C22. For panels A and C, the images were processed with a digital camera and NIH Image 1.57 software. The figures were produced with the program Canvas.

conformational change. Two other molecules that facilitate the conformational change were also identified. One (C29), however, was too toxic to determine its effect on infectivity, while the other (S23) had no measurable effect on infectivity (Table 1).

Further characterization of the effects of TBHQ and C22 on the low-pH-induced conformational change in HA. The low-pH-induced conformational change in HA is an irreversible event that is believed to be under kinetic control (2). Since TBHQ inhibits the conformational change while C22 appears to facilitate it, each compound might alter either the pH at which the conversion occurs or the time necessary to achieve the conversion (or both). To investigate these possibilities, we compared the effects of TBHQ and C22 on the time (Fig. 5A and C) and pH dependence (Fig. 5B and D) of the conformational change. As shown in Fig. 5, 100 μM TBHQ stabilizes BHA, while 100 μM C22 destabilizes it, with respect to both the time of exposure (Fig. 5A and C) and the pH (Fig. 5B and D) required to effect the conformational change. Preliminary studies indicated that C22 also potentiates the low-pH-induced conversion of HA to a form that is sensitive to proteinase K (21). As seen in Fig. 5D, C22 did not have any effect on the protease sensitivity of BHA at neutral pH and room temperature. The latter finding suggested that C22 does not inhibit

TABLE 1. Effects of compounds targeted to new DOCK sites

Compound	IC$_{50}$ (μM)[a]			Force field score[b]
	Conformational change	Infectivity	Cell viability	
TBHQ[c]	Inhibitor (12)	20.0	>100	−15.4
S19	Inhibitor (<100)	0.8	>>500	−38.1
S22	Inhibitor (<100)	40.0	>>100	−43.3
C22	Effector (8)	8.0	1,000	−41.9
S23	Effector (<100)	>100	100	−35.6
C29	Effector (<100)	ND[d]	<1	−43.0
S28	Inhibitor (<100)	>50	>50	−35.7
C13	Inhibitor (<100)	>100	>100	−41.1
C26	No effect	ND	ND	−39.8
S15	No effect	ND	ND	−35.1
S110	No effect	ND	ND	−36.7
C19	No effect	ND	ND	−40.9
S17	No effect	ND	ND	−34.6

[a] Effects on conformational change, infectivity, and cell viability were measured with the thermolysin, ELISA, and MTT assays, respectively, as described in Materials and Methods.

[b] Calculation of the DOCK force field score is as per the DOCK3.5 user's manual; a more negative value indicates a higher predicted affinity.

[c] Values for the effects of TBHQ on conformational change (SPA assay), infectivity, and cell viability are from reference 6.

[d] ND, not determined.

viral infectivity by inactivating the virus under neutral-pH conditions.

Effects of TBHQ and C22 on viral infectivity. The effect of TBHQ on influenza virus infectivity has been examined with both a single-cycle as well as a multiple-cycle infection assay (6, 41) (see Materials and Methods). The same methods were applied here to study the effects of C22 on viral infectivity. As seen in Fig. 6A, C22 inhibits infectivity in the single-cycle growth assay with an IC$_{50}$ of 8 μM; C22 is not toxic to MDCK2 cells at this or higher concentrations (Fig. 6A and Table 1). Similar results were obtained with the multiple-cycle infectivity assay (IC$_{50}$ of approximately 10 μM [data not shown]). We next investigated the time window during which TBHQ and C22 exert their effects. To do this, each inhibitor was added at various times during a single cycle of infection in MDCK2 cells and at 15 h postinfection, the culture medium was assayed for the amount of virus produced. As shown in Fig. 6B and C, each compound has a significant antiviral effect, but only if added early in the viral life cycle; the effect continues until 30 min postadsorption but then drops off precipitously at 1 h. The inhibitory effect of TBHQ disappears if the compound is added after this time. In the case of C22, however, a detectable antiviral effect remained at later times; the latter effect was more pronounced at higher concentrations of C22. Another experiment testing hemagglutination showed that viral adsorption (i.e., cell surface receptor binding) is not affected by 10 μM C22, but that 100 μM C22 inhibits viral adsorption by 50% (data not shown). TBHQ had no effect on hemagglutination at either concentration.

Effects of TBHQ and C22 on fusion. Since TBHQ and C22 affect the conformational change in HA and inhibit infectivity early in the viral life cycle, it is likely that they affect HA-mediated membrane fusion. We previously showed that TBHQ inhibits influenza virus-induced syncytium formation, suggesting that it inhibits membrane fusion (6). Here, we tested the effects of TBHQ and C22 on fusion by using a content-mixing assay. RBCs were preloaded with β-galactosidase and then bound to HA-expressing CHO cells. When the RBC-cell complexes are exposed to pH 5.0, the RBCs fuse with the CHO cells, delivering their contents to the CHO cell cytoplasm (25, 29). As seen in Table 2, both TBHQ and C22 inhibit RBC-cell fusion at 10 and 100 μM, the same range in which they inhibit conformational change and viral infectivity.

To investigate the effects of TBHQ and C22 on the pH dependence of membrane fusion, we used a hemolysis assay. This assay was used because the viral hemolytic activity reflects

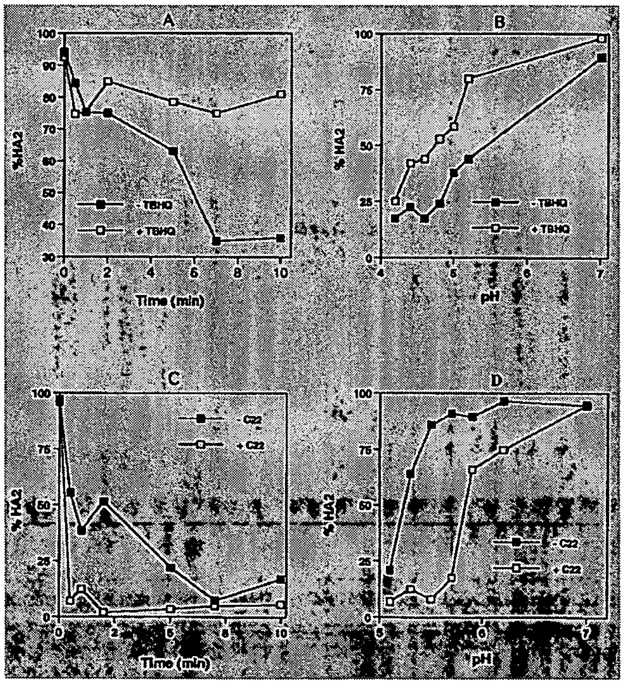

FIG. 5. Effect of TBHQ (A and B) and C22 (C and D) on the conformational change of HA: time (A and C) and pH (B and D) dependence. Samples of biotinylated BHA were treated without (solid squares) or with (open squares) 100 μM TBHQ (A and B) or C22 (C and D) and then incubated at pH 5.2 at room temperature for the indicated time (A and C) or incubated at the indicated pH for 7 min at room temperature (B and D). Following reneutralization, samples were analyzed for thermolysin sensitivity as described in the legend to Fig. 4 and in Materials and Methods.

both the fusion activity and the conformational change in HA (11, 23). In addition, the assay is easy to perform and quantitate. The inhibitory effects of TBHQ and its relatives on hemolysis by HA have been reported previously (see Table 4 and Fig. 7 of reference 6). As shown in Fig. 7, C22 (10 μM) inhibits hemolysis in the same pH range at which it facilitates the conformational change (Fig. 5D); the effect presumably remains at lower pH values, but the assay is affected by decreasing hemolytic efficiency at pH values approaching and below 5.0 (6). At pH 5.6, the IC_{50}s for C22 in the hemolysis assay ranged between 10 and 25 μM in different experiments. With 10 μM C22, the extent of inhibition (at pH 5.6) ranged between 28 and 49%. A 100 μM concentration of C22 inhibits hemolysis more effectively than does 10 μM C22, but this higher concentration of inhibitor was found to decrease virus-RBC binding, while 10 μM C22 did not (data not shown).

Mutants resistant to TBHQ and C22. We isolated and characterized seven TBHQ-resistant influenza variants. Table 3 lists each isolate, the HA residues mutated, and their sensitivities to TBHQ compared to those of wild-type virus. When mapped onto the neutral-pH crystal structure of X:31 BHA (46), the mutations clustered in two regions: in the vicinity of the fusion peptide and in the globular head domain interface (Fig. 8A), a distribution strikingly similar to that of mutations conferring resistance to high doses of amantadine (11, 39). As expected, all of the resistant isolates were destabilized with respect to the pH at which their HA changes conformation (Table 3) as measured by a hemolysis assay using intact virus (11). Five mutations occur at residues that in wild-type virus, make interactions with the fusion peptide (11, 39, 47); these mutations likely allow the fusion peptide to become exposed more easily, thereby facilitating the conformational change and subsequent fusion (11). Four of the mutations that we identified in the fusion peptide region, HA2 D112E, D112N, D109G, and K117E, were the same as those in previously identified amantadine-resistant mutants (39). A fifth mutation, T111A, occurs in the same region as these others but was not identified as a high-dose amantadine resistance mutation. It occurs in a double mutation with HA1 P103K; the latter residue is found in the intermonomer region between the heads of HA, which are known to separate during the conformational change (18, 24). Another mutation, HA1 A198E, maps to the interface region of the heads. Both of these mutations in the head domain (HA1 A198E and HA1 P103K) occur near, but not at the same loci as, the sites of previously identified amantadine-resistance mutations. The double mutant containing the HA1 P103K HA2 T111A mutation was shown to be destabilized with respect to the pH at which it undergoes the conformational change (Table 3), while the isolate with the mutation HA1 A198E was not detectably destabilized. The final mutation, HA2 R124G, occurs well away from the fusion peptide and even farther from the heads in the neutral structure (Fig. 8A). This mutation also destabilizes HA with respect to pH

TABLE 2. Effect of TBHQ and C22 on fusion between CHO cells expressing HA and erythrocyte ghosts containing β-galactosidase[a]

Inhibitor concn[b] (μM)	HA type[c]	pH[d]	No. of fusions/field[e]	% Fusion[f]
None	HA	5	20 ± 2	100
	HA0	5	0	0
	HA0	7	0	0
	HA	7	0	0
C22				
10 μM	HA	5	10 ± 3	51
100 μM	HA	5	1 ± 1	6
100 μM	HA0	5	0	0
100 μM	HA	7	0	0
TBHQ				
10 μM	HA	5	9 ± 2	45
100 μM	HA	5	5 ± 2	25
100 μM	HA0	5		0
100 μM	HA	7	0	0

[a] Assay was performed as described in Materials and Methods.

[b] Concentration of compound present during incubations.

[c] Where indicated, cells were pretreated with trypsin to cleave the inactive precursor HA0 into active HA.

[d] RBC-cell complexes were treated at the indicated pH for 2 min at room temperature.

[e] Number of nuclei in fused areas (blue) per field at ×100 magnification (a measure of fusion activity). Results are averaged from two assays.

[f] Percentage of fusion compared to no inhibitor.

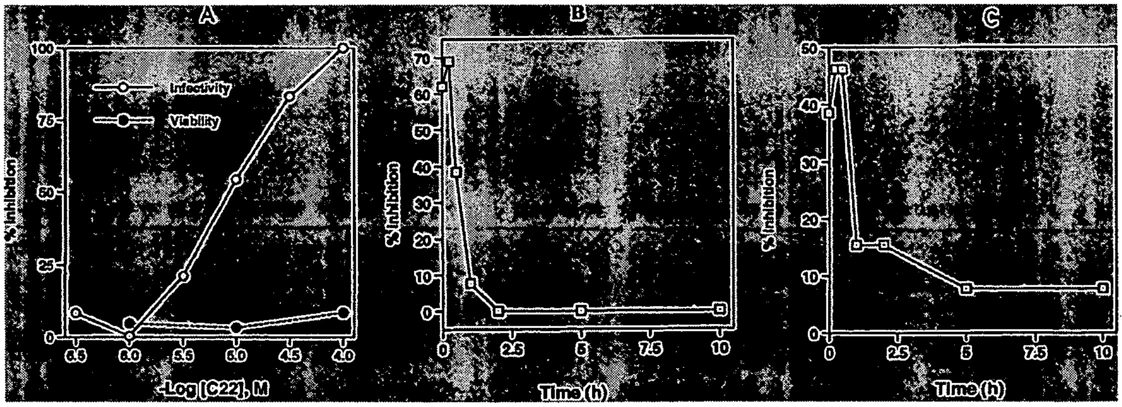

FIG. 6. (A) Effect of C22 on infectivity and cell viability. Infectivity was measured for a single cycle with an ELISA, and cell viability was monitored in parallel by assaying for metabolism of MTT, as described in Materials and Methods. Open circles, infectivity; solid circles, cell viability. (B and C) Effects of TBHQ (B) and C22 (C) when added at various times during a viral infection cycle. The single-cycle infectivity assay was performed as described in Materials and Methods. Virus was prebound to MDCK2 cells at 4°C, the cells were washed, and prewarmed (37°C) medium was added to initiate infection. TBHQ (B) or C22 (C) (10 μM [each]) was added at the indicated times during a single cycle of influenza virus infection, and the amount of virus produced was assessed by plaque assay at 15 h postinfection, the time required to complete a single cycle of infection (16). Control experiments showed no effect of these inhibitors (at the concentrations tested) on virus-receptor binding (data not shown).

(Table 3), and it occurs at the site of an intermonomer salt bridge in wild-type virus with aspartate HA2 132 (Fig. 8B). A charge-reversal mutation at HA2 132 was identified earlier in a virus that induces fusion at a relatively elevated pH (13), and the mutation at HA2 124 presumably has the same effect.

We also isolated and characterized two virus variants that are approximately 10-fold resistant to C22 (Table 4). Both resistant mutants lyse RBCs at a lower pH than wild-type virus does (Table 4), suggesting that both mutants are stabilized with respect to the pH at which their HA converts to the fusogenic form. Figure 8C shows the locations of the residues mutated in the C22-resistant isolates in the context of the crystal structure of native, wild-type BHA (46). The mutation HA1 S219P occurs in the head region, perhaps altering the position of a β-strand that contains intermonomer contacts and allowing new contacts to form. The second mutation, HA1 K27E, was isolated four times independently. Figure 8D shows the area surrounding HA1 K27 in the native structure. This residue lies on the interface between monomers and places a positive charge very close to another positive charge on a neighboring residue (HA2 54 of another HA monomer); the mutation from lysine to glutamate presumably allows an intermonomer salt link to be formed, further stabilizing the interface (see Discussion).

We reasoned that a virus that is destabilized with respect to the pH of its conformational change would be more sensitive to C22 than the wild-type virus is. To test this hypothesis, we assessed the sensitivity of the HA2 R124G mutant, which is highly resistant to TBHQ (Table 3), for its sensitivity to C22. Based on a plaque assay analysis, the HA2 R124G mutant is approximately 2.3-fold more sensitive to C22 than is wild-type virus (Table 4).

Since the low-pH conformational change in HA is irreversible (50), if C22 inhibits infectivity by facilitating this change, the inhibition should be irreversible. To examine this possibility, virus was incubated with 10 μM C22, and the pH was lowered to various pH values. The pH values selected have been shown to allow nearly the entire HA population to change conformation in the presence of C22 (pH 5.8, 5.6, and 5.4 [Fig. 5D and 7]), while only a portion changes in its absence (Fig. 5D and 9) (37). As seen in Fig. 9, C22 irreversibly inhibits viral infectivity under these conditions. This is in distinct contrast to TBHQ, which is a reversible inhibitor (Fig. 9).

DISCUSSION

Mechanism of TBHQ inhibition of infectivity. TBHQ was originally identified as an inhibitor of fusion peptide exposure (6). The concurrence of the IC_{50} values for inhibition of both fusion and viral infectivity suggested a causal relationship. In this paper, we have described several lines of evidence that further support this mechanism of TBHQ inhibition of influenza virus infection. First, the striking similarity between the HA mutations in TBHQ-resistant and high-dose amantadine-resistant viruses indicates a shared mode of action. It has been shown that the concentration of amantadine used to isolate these earlier mutants (100 μg/ml) raises the pH of intracellular

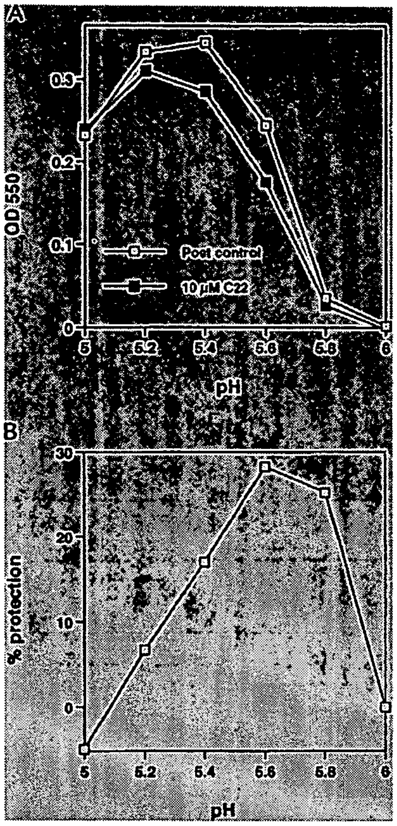

FIG. 7. (A) Effect of C22 on hemolysis. Whole, washed erythrocytes were incubated with (solid squares) or without (open squares) 10 μM C22 and virus and treated at the indicated pH for 15 min at room temperature before being analyzed for hemolysis as described in Materials and Methods. OD 550, optical density at 550 nm. (B) Percent difference between the curves in panel A indicating the pH range over which C22 inhibits hemolysis. In the experiment shown, the inhibition by C22 at pH 5.6 was 28%. This value ranged from 28 to 49% in different experiments. Inhibition at pH 5.8 (~25%) was consistently observed in eight separate experiments.

TABLE 3. HA mutations in TBHQ-resistant viruses

Mutant residue[a]	Mutant IC_{50}/wild-type IC_{50}[b]	Shift in pH of hemolysis (reference)[c]	Amantadine resistance[d]
HA2 D112E	10	0.4 (39)	Yes
HA2 D112N	2	0.4 (39)	Yes
HA2 D109G	2	0.1 (39)	Yes
HA2 K117E	10	0.4 (39)	Yes
HA2 R124G	11	0.3 (This work)	No
HA1 P103K HA2 T111A	3	0.1 (This work)	No
HA1 A198E	7	None detected (This work)	No

[a] Each entry indicates the mutation(s) in a single isolate. Note the presence of a mutant with a double mutation (HA1 P103K HA2 T111A).

[b] Values represent fold difference in IC_{50} compared with IC_{50} of wild-type (X:31) virus.

[c] Shift in pH at which 50% hemolysis occurs compared with hemolysis in the wild-type virus.

[d] Presence of mutations identified previously in X:31 viruses resistant to high concentrations of amantadine (39).

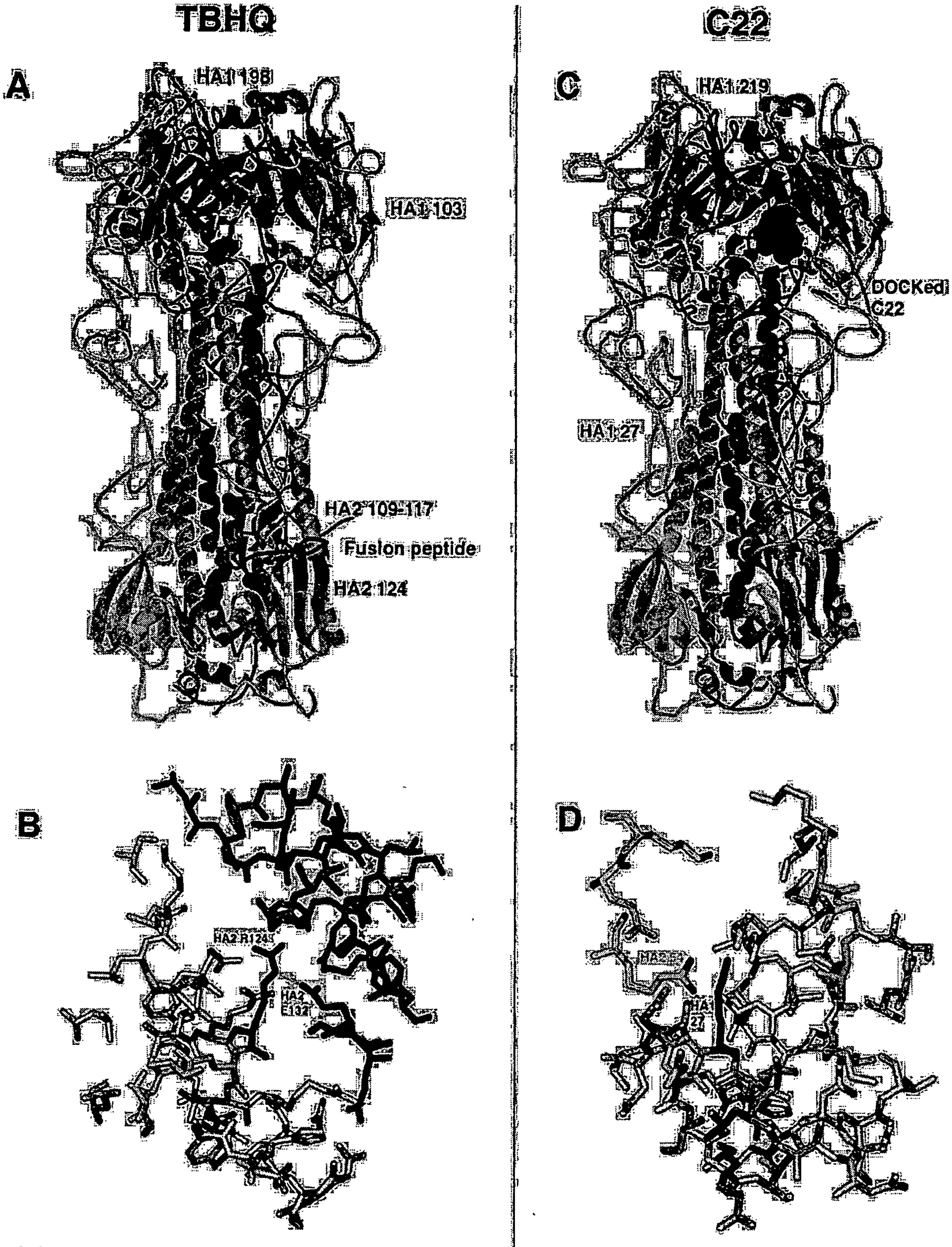

FIG. 8. Mutations in HAs of inhibitor-resistant influenza viruses. (A) Locations of HA mutations in TBHQ-resistant influenza viruses. BHA is shown in its neutral-pH form as in Fig. 2. The fusion peptide of one monomer is shown in black. Wild-type residues mutated in TBHQ-resistant isolates are indicated in magenta as CPK-rendered side chains. (B) Protein residues surrounding the residue HA2 R124 (magenta), which is mutated to Gly in a TBHQ-resistant isolate. BHA monomers are colored as in panel A. (C) HA mutations in C22-resistant isolates. Mutated residues are indicated by their wild-type side-chains as in panel A. Blue space-filling model, DOCK-selected orientation of C22 in site 2A. (D) Close-up of area surrounding HA1 K27.

TABLE 4. Sensitivity of HA mutants to C22

Mutant residue no.[a]	Selection[b]	Sensitivity to C22 vs. wild type[c]	Shift in pH of hemolysis
HA1 219	C22	10-fold lower	−0.3
HA1 27	C22	10-fold lower	−0.6
HA2 124	TBHQ	2.3-fold higher	+0.25

[a] Mutation in HA.

[b] Method of isolate selection. Each entry indicates virus was selected for resistance to C22 or TBHQ.

[c] IC_{50} infectivity for each isolate was measured in the presence of 0.1 to 100 μM C22 by plaque assay.

vesicles to levels incompatible with the conformational change of wild-type HA (11). Furthermore, the amantadine-resistant viral isolates possess mutations that destabilize HA with respect to pH, indicating that the drug was acting to inhibit the HA conformational change (11, 39). The same is true for the TBHQ-resistant mutants isolated in this study. The use of TBHQ to select destabilized HA mutants is, however, more specific than the use of high doses of amantadine. Amantadine does not interact directly with BHA (5), and, moreover, given that the drug directly inhibits the virus proton channel M2 (48), it is likely to have pleiotropic effects at high concentrations. The HAs of all of the TBHQ-resistant mutants are detectably destabilized with respect to pH except for one: that of the mutant with the HA1 A198E mutation. It is not yet clear how this mutation leads to resistance, since it does not destabilize HA, nor does it lie near the presumed binding site. This case aside, the finding that the other six virus isolates resistant to TBHQ all have HAs that change conformation at an elevated pH indicates that TBHQ acts to stabilize HA during the course of an infection and that this stabilization impedes infectivity.

Another line of evidence that TBHQ acts by inhibiting the conformational change in HA is that it only inhibits viral infectivity (at its IC_{50} [see below]) if added during the first 15 to 30 min of infection. This time dependence places the level of action at the earliest portions of the influenza virus life cycle, namely cell surface binding, endocytosis, or membrane fusion.

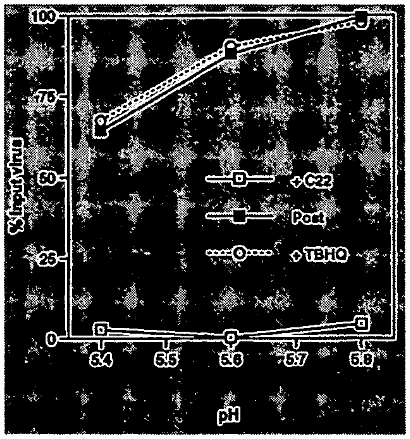

FIG. 9. C22 irreversibly inhibits viral infectivity. X:31 virus was treated with 10 μM C22 (open squares) or TBHQ (open circles) for 25 min at room temperature. The pH was then lowered to the indicated value for 7 min at room temperature and reneutralized. "Post" control experiments (solid squares) were performed in which C22 was added after reneutralization. Samples were then diluted 100-fold and analyzed for infectivity by ELISA as described in Materials and Methods.

Earlier observations have demonstrated that fusion of influenza virus occurs between 25 and 30 min after cell binding (38). TBHQ does not inhibit receptor binding (Fig. 6), strongly suggesting that its inhibitory action is at the level of fusion.

Finally, the fusion assays presented here directly demonstrate that TBHQ inhibits fusion between erythrocyte ghosts and cells expressing the X:31 influenza virus HA. Taken together, the above evidence strongly suggests that TBHQ inhibits influenza virus infectivity by the mechanism for which it was selected: inhibition of membrane fusion by the stabilization of an inactive form of HA.

Several recent studies have shed light on the virus subtype specificity of TBHQ. One recent report used the hydrophobicity probe bis-ANS to confirm inhibition of the low-pH conformational change in X:31 HA (subtype H3) by TBHQ (4). Another study, however, has shown that TBHQ has no effect on the kinetics of fusion by influenza virus of the H1 subtype (32). Furthermore, we have shown that the antiviral effect of TBHQ is diminished against influenza virus of the H2 subtype and that the conformational change of BHA from an H2 virus is not inhibited by TBHQ (21). More recently, a compound bearing some molecular similarity to TBHQ, termed BMY-27709, was identified that inhibits hemolysis and infection by H1 and H2 viruses but not by H3 viruses (28). A mutant virus resistant to BMY-27709 contains an amino acid change at HA2 110, which is predicted to be located near several of the mutations in TBHQ-resistant H3 viruses that we isolated (Fig. 8A). Although the study reporting BMY-27709 hypothesized that the occurrence of a mutation at HA2 110 in a virus resistant to BMY-27709 suggested that the binding site for BMY-27709 is near this residue, this need not be the cause. The proximity of HA2 110 to mutations found in virus isolates resistant to both TBHQ (this study) and to amantadine (11) suggests that all of these mutations allow HA to change conformation at an elevated pH and thus confer resistance to agents that stabilize the protein's native conformation.

Evaluation of the inhibitor design method. Since the identification of TBHQ as an inhibitor of the fusion-inducing conformational change in the influenza virus HA (6), there have been several improvements that encouraged further development of our structure-based inhibitor design strategy. (i) The DOCK program was improved (19, 30). (ii) The resolution of the BHA structure increased from 3 Å to 2.1 Å (44). (iii) Recent studies have given new insight into the mechanism of fusion peptide exposure. Examples of such information are the need for motion in the HA1 globular head domains (18, 24) and a loop-to-helix transition of HA2 54–81 (7, 8, 30a). We therefore used the refined DOCK in conjunction with the higher-resolution BHA structure to perform structure-based inhibitor searches targeting the region of HA that undergoes the loop-to-helix transition. As a result of this computational analysis, we tested 12 small molecules for their effect on the low-pH conformational change and viral infectivity. We consider it significant that out of the 12 small molecules tested, 7 have an effect on the conformational change at micromolar concentrations. In comparison, 43 molecules were tested before a lead inhibitor (IC_{50} of 500 μM) was identified in the original search (6). In addition to the improvement in the "hit rate," the first-round hits found in the new search are more potent than those identified in the earlier work. In fact, the most potent of the new first-round inhibitors (S19) is more potent than is TBHQ, the best second-round derivative from the earlier search, and the potency of the best first-round new inhibitors is about the same as that of the second-round old ones (both low-micromolar IC_{50}s). Although certainly not conclusive, our findings suggest that the search with the recent version of DOCK (DOCK3.5) (19, 30) and the improved BHA structure (44) has been more successful at selecting molecules that bind to the sites to which they were targeted than the search with an earlier version of DOCK (DOCK2) (34) and the lower-resolution BHA structure (6). X-ray crystallographic examination of the interaction of BHA with TBHQ and the new inhibitors is necessary to clarify this issue.

C22 is an effector of the conformational change in HA. As a consequence of our new DOCK search, we identified an effector of the low-pH-induced conformational change that inhibits influenza virus infectivity. Although this was not a specific goal, the effect of this compound was not entirely unanticipated, since it has been known for some time that if X:31 influenza virus is pretreated at low pH in the absence of a target membrane, it is irreversibly inactivated for fusion (37). Examination of the DOCK sites analyzed in this search (Fig. 2) reveals many intermonomer contacts that could be either stabilized or destabilized by a small molecule. In addition, the interfaces consist partially of hydrophobic surfaces; an amphipathic molecule could possibly bind to one of these surfaces during the conformational change, lowering the energy barrier of the conversion to the low-pH form by shielding the surface from exposure to solvent. As a result of our search, we identified three compounds that potentiate the conformational change. It was not clear at the outset, however, that these compounds would inhibit fusion and infectivity. In fact, since C22 does not induce the conformational change at neutral pH, it was conceivable that it might facilitate fusion. One main fact argued against the latter possibility: Influenza viruses display a pH optimum of fusion; below this pH value, the efficiency of fusion decreases (13, 26). Presumably, the effect of very low pH is similar to the presence of an effector such as C22, in that it decreases the efficiency of fusion through its effect on HA (Fig. 5D and 7 and Table 2).

Our results indicate that C22 destabilizes HA (Fig. 3C and 4C and D) and also inhibits hemolysis and fusion (Fig. 7 and Table 2) and viral infectivity (Fig. 6). In fact, the pH range over which C22 inhibits hemolysis most effectively, pH 5.2 to 5.8, closely mirrors the range in which it facilitates the conformational change. There are at least three possible explanations for the behavior of C22. (i) C22 induces an excessively rapid conformational change in HA which inactivates HA, thereby depleting the pool of fusion-active trimers and inhibiting fusion. (ii) In a variant of explanation i, C22 causes HA to convert to a fusion-inactive conformation that is distinct from the low-pH conformation represented by TBHA2 (7). This possibility could explain the (additional) late effect of C22 in the viral life cycle (Fig. 6C); as HA is being synthesized and processed in the endoplasmic reticulum, C22 may unfold HA, causing the production of defective viruses. (This effect would have to be on uncleaved HA [HA0], since MDCK2 cells do not cleave HA0 into HA1 and HA2 [41].) Support for this hypothesis comes from the observation that for HAs that can be cleaved during biosynthesis, alteration of the pH of vesicles containing newly produced HA with the drug amantadine leads to the production of noninfectious virus particles (40). (iii) The final mechanism supposes that even though C22 has not been shown to cause conformational changes in HA at neutral pH (Fig. 5D), C22 may allow HA to become inactivated thermally or by other conditions during the course of an infection. This possibility was put forth for viruses with mutations that destabilize their HAs (11). With any of these mechanisms, the effect would be irreversible (unlike that of TBHQ and its relatives, which have a reversible inhibitory effect on HA) (6) (Fig. 9). Indeed, C22 is an irreversible inhibitor of viral infectivity (Fig. 9).

Support for the hypothesis that C22 inhibits viral fusion and infectivity by destabilizing HA comes from the location of mutations in viruses resistant to C22: HA1 A219P and HA1 K27E. For both of the mutants carrying these mutations, the pH dependence of the conformational change in HA is shifted (0.3 and 0.6 pH units, respectively) in a more acidic direction than that of wild-type HA (Table 4). Heretofore, the only known mutation that demonstrated such a stabilizing effect was HA2 K58I (40). The mutation at HA1 27 likely involves removal of an intermonomer charge repulsion with the arginine residue at HA2 54 (Fig. 8D). Moreover, the substitution of a glutamate at position 27 likely allows for the formation of a stabilizing salt bridge with HA2 R54. The segment of HA on which HA2 27 is found (HA1 14–52) in neutral-pH HA has been shown previously to move very early during the conformational change (51) and crosses the region of HA2 that undergoes a helix-to-loop transition at low pH (HA2 106–112) (7). Hence, HA1 14–52 could be critical in tethering the trimer in the fusion-inactive conformation. Furthermore, both HA2 54 and 58 lie within the portion of HA2 that undergoes a loop-to-helix transition at low pH (7, 8); recent evidence has demonstrated the role of this area in regulating HA-mediated membrane fusion (30a). Finally, the relatively higher sensitivity of the isolate with the mutation HA2 R124G, which has a destabilized HA, to C22 compared to that of the wild type offers more support for the proposed mechanism of C22. Crystallographic analysis of the C22-resistant mutants could shed light on the control of the HA conformational change.

C22 was designed and shown to be effective against HA from the X:31 strain of influenza virus (H3 subtype). In preliminary experiments, we have found that C22 also inhibits the hemolytic activity of A/Victoria influenza virus (H3 subtype) as well as A/Japan/305 influenza virus (H2 subtype), albeit with different apparent potencies. Future work is necessary to determine the spectrum of activity of C22 against different influenza viruses. On the other hand, the effect of C22 appears to be specific for influenza virus HA; 100 μM C22 had no effect on cell-cell fusion mediated by the human immunodeficiency virus (HIV) envelope glycoprotein (19a).

Premature triggering of the fusion-inducing conformational change. Premature triggering of the conformational change in HA from X:31 influenza virus is irreversible (37) (Fig. 9). Hence, irreversible facilitators of the conformational change, such as C22, offer a distinct advantage over reversible inhibitors of the conformational change, such as TBHQ and S22. Although C22 itself does not appear to be able to trigger the conformational change in HA at neutral pH, it may be possible to identify small molecules that would. A facilitator that functions at neutral pH would offer the additional advantage of being able to act outside of the cell, a more pharmacologically tractable site for intervention than the endocytic compartment, where C22 appears to act. In the case of influenza virus, it may be possible to design a variant of C22 that would have this feature.

Currently, only two closely related anti-influenza virus drugs are approved for clinical use in the United States: amantadine and rimantadine. Both act by inhibiting a viral ion channel, but they cause undesirable side effects (55) and are plagued by clinical resistance (22, 31, 55). Two promising new drugs, 4-guanidino-Neu5Ac2en (4-GuDANA) and GS4104, were designed to inhibit the viral enzyme neuraminidase (56), and they are currently being evaluated for clinical use (31), but resistance to at least one of these neuraminidase inhibitors has already been encountered in laboratory settings (31, 36). New inhibitors of the ion channel activity of the viral M2 protein (43) and of the viral polymerase (42) have only recently been identified. Drugs that inhibit HA-mediated membrane fusion would thus be a welcome addition to the anti-influenza virus armamentarium.

It may also be possible to discover or design inhibitors or facilitators of the conformational changes in the fusion proteins of other enveloped viruses such as rabies virus, HIV, and Ebola virus. Peptides have already been identified that specifically inhibit fusion of HIV and paramyxoviruses; these peptides are composed of sequences from regions of the HIV Env and the paramyxovirus F proteins that are believed to be analogous to HA2 54–81 (27, 52). It remains to be seen exactly how these peptides inhibit fusion, but it is possible that they somehow affect a conformational change. Work with the envelope glycoprotein of another retrovirus, avian sarcoma and leukosis virus, has shown that binding of soluble cell receptor to Env renders the viral protein sensitive to thermolysin (17) in a manner reminiscent of the effect of low pH on HA; this soluble receptor has also been shown to inhibit viral entry into cells (9). In conclusion, the results that we have presented here for both the inhibitors and facilitators of the conformational change in HA suggest that the strategy of either stabilizing or prematurely triggering viral fusion proteins could be applied to other enveloped viruses.

ACKNOWLEDGMENTS

We thank Don Ganem for his generous support and for many helpful discussions and Paul Straight for technical assistance.

This work was supported by NIH grants GM31497 (I.D.K.) and AI22470 (J.M.W.). L.R.H. was supported by the Medical Scientist Training Program of the University of Calif., San Francisco.

REFERENCES

1. **Ausubel, F. M., R. Brent, R. E. Kingston, D. D. Moore, J. G. Seidman, J. A. Smith, and K. Struhl.** 1995. Short protocols in molecular biology. John Wiley & Sons, Inc., New York, N.Y.
2. **Baker, D., and D. A. Agard.** 1994. Influenza hemagglutinin: kinetic control of protein function. Structure 2:907–910.
3. **Bernstein, F. C., T. F. Koetzle, G. J. B. Williams, J. Meyer, E. F., M. C. Brice, J. R. Rodgers, O. Kennard, T. Shimanouchi, and M. Tasumi.** 1977. The protein data bank: a computer-based archival file for macromolecular structures. J. Mol. Biol. 112:535–542.
4. **Bethell, R. C., N. M. Gray, and C. R. Penn.** 1995. The kinetics of the acid-induced conformational change of influenza virus haemagglutinin can be followed using 1,1′-bis(4-anilino-5-naphthalenesulphonic acid). Biochem. Biophys. Res. Commun. 206:355–361.
5. **Bodian, D.** 1992. Ph.D. thesis. University of California, San Francisco.
6. **Bodian, D. L., R. B. Yamasaki, R. L. Buswell, J. F. Stearns, J. M. White, and I. D. Kuntz.** 1993. Inhibition of the fusion-inducing conformational change of influenza hemagglutinin by benzoquinones and hydroquinones. Biochemistry 32:2967–2978.
7. **Bullough, P. A., F. M. Hughson, J. J. Skehel, and D. C. Wiley.** 1994. Structure of influenza haemagglutinin at the pH of membrane fusion. Nature 371:37–43.
8. **Carr, C. M., and P. S. Kim.** 1993. A spring-loaded mechanism for the conformational change of influenza hemagglutinin. Cell 73:823–832.
9. **Connolly, L., K. Zingler, and J. A. T. Young.** 1994. A soluble form of a receptor for subgroup A avian leukosis and sarcoma viruses (ALSV-A) blocks infections and binds directly to ALSV-A. J. Virol. 68:2760–2764.
10. **Daniels, R. S., A. R. Douglas, J. J. Skehel, M. D. Waterfield, I. A. Wilson, and D. C. Wiley.** 1983. Studies of the influenza virus haemagglutinin in the PH5 conformation, p. 1–7. *In* W. G. Laver (ed.), The origin of pandemic influenza viruses. Elsevier Science Publishing Co., Inc., New York, N.Y.
11. **Daniels, R. S., J. C. Downie, A. J. Hay, M. Knossow, J. J. Skehel, M. L. Wang, and D. C. Wiley.** 1985. Fusion mutants of the influenza virus hemagglutinin glycoprotein. Cell 40:431–439.
12. **DesJarlais, R., R. Sheridan, G. Seibel, J. Dixon, I. Kuntz, and R. Venkataraghavan.** 1988. Using shape complementarity as an initial screen in designing ligands for a receptor binding site of known three-dimensional structure. J. Med. Chem. 31:722–729.
13. **Doms, R. W., M.-J. Gething, J. Henneberry, J. White, and A. Helenius.** 1986. Variant influenza virus hemagglutinin that induces fusion at elevated pH. J. Virol. 57:603–613.
14. **Ellens, H., S. Doxsey, J. S. Glenn, and J. M. White.** 1989. Delivery of macromolecules into cells expressing a viral membrane fusion protein. Methods Cell Biol. 31:155–176.
15. **Ferrin, T. E., C. C. Huang, L. E. Jarvis, and R. Langridge.** 1988. The Midas display system. J. Mol. Graphics 6:13–27.
16. **Gaush, C. R., and T. F. Smith.** 1968. Replication and plaque assay of influenza virus in an established line of canine kidney cells. Appl. Microbiol. 16:588–594.
17. **Gilbert, J. M., L. D. Hernandez, J. W. Balliet, P. Bates, and J. M. White.** 1995. Receptor-induced conformational changes in the subgroup A avian leukosis and sarcoma virus envelope glycoprotein. J. Virol. 69:7410–7415.
18. **Godley, L., J. Pfeifer, D. Steinhauer, B. Ely, G. Shaw, R. Kaufmann, E. Suchanek, C. Pabo, J. J. Skehel, D. C. Wiley, and S. Wharton.** 1992. Introduction of intersubunit disulfide bonds in the membrane-distal region of the influenza hemagglutinin abolishes membrane fusion activity. Cell 68:635–645.
19. **Gschwend, D., and I. Kuntz.** 1996. Orientational sampling and rigid-body minimization in molecular docking revisited: on-the-fly optimization and degeneracy removal. J. Comput.-Aided Mol. Des. 10:123–132.

19a. **Hernandez, L., and J. M. White.** Unpublished observations.

20. **Hernandez, L. D., L. R. Hoffman, T. G. Wolfsberg, and J. M. White.** 1996. Virus-cell and cell-cell fusion. Annu. Rev. Cell Dev. Biol. 12:627–661.
21. **Hoffman, L.** 1996. Ph.D. thesis. University of California, San Francisco.
22. **Houck, P., M. Hemphill, S. LaCroix, D. Hirsch, and N. Cox.** 1995. Amantadine-resistant influenza A in nursing homes. Identification of a resistant virus prior to drug use. Arch. Intern. Med. 155:533–537.
23. **Huang, R. T. C., R. Rott, and H.-D. Klenk.** 1981. Influenza viruses cause hemolysis and fusion of cells. Virology 110:243–247.
24. **Kemble, G. W., D. L. Bodian, J. Rosé, I. A. Wilson, and J. M. White.** 1992. Intermonomer disulfide bonds impair the fusion activity of influenza virus hemagglutinin. J. Virol. 66:4940–4950.
25. **Kemble, G. W., T. Danieli, and J. M. White.** 1994. Lipid-anchored influenza hemagglutinin promotes hemifusion, not complete fusion. Cell 76:383–391.
26. **Krumbiegel, M., A. Hermann, and R. Blumenthal.** 1994. Kinetics of the low pH-induced conformational changes and fusogenic activity of the influenza hemagglutinin. Biophys. J. 67:2355–2360.
27. **Lambert, D., S. Barney, A. Lambert, K. Guthrie, R. Medinas, D. Davis, T. Bucy, J. Erickson, G. Merutka, and S. J. Pettesay.** 1996. Peptides from conserved regions of paramyxovirus fusion (F) proteins are potent inhibitors of viral fusion. Proc. Natl. Acad. Sci. USA 93:2186–2191.
28. **Luo, G., R. Colonno, and M. Krystal.** 1996. Characterization of a hemagglutinin-specific inhibitor of influenza A virus. Virology 226:66–76.
29. **Melikyan, G. B., J. M. White, and F. S. Cohen.** 1995. GPI-anchored influenza hemagglutinin induces hemifusion to both red blood cell and planar bilayer membranes. J. Cell Biol. 131:679–691.
30. **Meng, E., B. Shoichet, and I. Kuntz.** 1992. Automated docking with grid-based energy evaluation. J. Comp. Chem. 13:505–524.

30a. **Qiao, H., S. Pelletier, L. Hoffman, J. Hacker, and J. White.** Submitted for publication.

31. **Service, R.** 1997. Researchers seek new weapon against the flu. Science 275:756–757.
32. **Shangguan, T., D. Alford, and J. Bentz.** 1996. Influenza virus-liposome lipid mixing is leaky and largely insensitive to the material properties of the target membrane. Biochemistry 35:4956–4965.
33. **Shoichet, B., D. Bodian, and I. Kuntz.** 1992. Molecular docking using shape descriptors. J. Comp. Chem. 13:380–397.
34. **Shoichet, B., and I. Kuntz.** 1991. Protein docking and complementarity. J. Mol. Biol. 221:327–346.
35. **Skehel, J. J., P. M. Bayley, E. B. Brown, S. R. Martin, M. D. Waterfield, J. M. White, I. A. Wilson, and D. C. J. Wiley.** 1982. Changes in the conformation of influenza virus hemagglutinin at the pH optimum of virus-mediated membrane fusion. Proc. Natl. Acad. Sci. USA 79:968–972.
36. **Staschke, K. A., J. M. Colacino, A. J. Baxter, G. M. Air, A. Bansal, W. J. Hornback, J. E. Munroe, and W. G. Laver.** 1995. Molecular basis for the resistance of influenza viruses to 4-guanidino-Neu5Ac2en. Virology 214:642–646.
37. **Stegmann, T., F. P. Booy, and J. Wilschut.** 1987. Effects of low pH on influenza virus. Activation and inactivation of the membrane fusion capacity of the hemagglutinin. J. Biol. Chem. 262:17744–17749.
38. **Stegmann, T., W. Morselt, J. Scholma, and J. Wilschut.** 1987. Fusion of influenza virus in an intracellular acidic compartment measured by fluorescence dequenching. Biochim. Biophys. Acta 904:165–170.
39. **Steinhauer, D. A., N. K. Sauter, J. J. Skehel, and D. C. Wiley.** 1992. Receptor binding and cell entry by influenza viruses. Semin. Virol. 3:91–100.
40. **Steinhauer, D. A., S. A. Wharton, J. J. Skehel, D. C. Wiley, and A. J. Hay.** 1991. Amantadine selection of a mutant influenza virus containing an acid-stable hemagglutinin glycoprotein: evidence for virus-specific regulation of the pH of glycoprotein transport vesicles. Proc. Natl. Acad. Sci. USA 88:11525–11529.
41. **Tobita, K., A. Sugiura, C. Enomoto, and M. Furuyama.** 1975. Plaque assay and primary isolation of influenza A viruses in an established line of canine kidney cells (MDCK) in the presence of trypsin. Med. Microbiol. Immunol. 162:9–14.
42. **Tomassini, J. E., M. E. Davies, J. C. Hastings, R. Lingham, M. Mojena, S. L. Raghoobar, S. B. Singh, J. S. Tkacz, and M. A. Goetz.** 1996. A novel antiviral

agent which inhibits the endonuclease of influenza viruses. Antimicrob. Agents Chemother. 40:1189–1193.

43. **Tu, Q., L. H. Pinto, G. Luo, M. Shaughnessy, D. Mullaney, S. Kurtz, M. Krystal, and R. Lamb.** 1996. Characterization of inhibition of M_2 ion channel activity by BL-1743, a novel inhibitor of influenza A virus. J. Virol. 70:4246–4252.
44. **Watowich, S. J., J. J. Skehel, and D. C. Wiley.** 1994. Crystal structures of influenza virus hemagglutinin in complex with high-affinity receptor analogs. Structure 2:719–731.
45. **Weber, T., G. Paesold, R. Mischler, G. Semenza, and J. Brunner.** 1994. Evidence for H^+-induced insertion of the influenza hemagglutinin HA2 N-terminal segment into the viral membrane. J. Biol. Chem. 269:18353–18358.
46. **Weis, W. I., A. T. Bruenger, J. J. Skehel, and D. C. Wiley.** 1990. Refinement of the influenza virus hemagglutinin by simulated annealing. J. Mol. Biol. 212:737–761.
47. **Weis, W. I., S. C. Cusack, J. H. Brown, R. W. Daniels, J. J. Skehel, and D. C. Wiley.** 1990. The structure of a membrane fusion mutant of the influenza virus haemagglutinin. EMBO J. 9:17–24.
48. **Wharton, S. A., R. B. Belshe, J. J. Skehel, and A. J. Hay.** 1994. Role of virion M2 protein in influenza virus uncoating: specific reduction in the rate of membrane fusion between virus and liposomes by amantadine. J. Gen. Virol. 75:945–948.
49. **Wharton, S. A., L. J. Calder, R. W. H. Ruigrok, J. J. Skehel, D. A. Steinhauer, and D. C. Wiley.** 1995. Electron microscopy of antibody complexes of influenza virus haemagglutinin in the fusion pH conformation. EMBO J. 14:240–246.
50. **White, J. M.** 1994. Fusion of influenza virus in endosomes: role of the hemagglutinin, p. 281–301. *In* E. Wimmer (ed.), Cellular receptors for animal viruses. Cold Spring Harbor Laboratory Press, Cold Spring Harbor, N.Y.
51. **White, J. M., and I. A. Wilson.** 1987. Anti-peptide antibodies detect steps in a protein conformational change: low-pH activation of the influenza virus hemagglutinin. J. Cell Biol. 105:2887–2896.
52. **Wild, C. T., D. C. Shugars, T. K. Greenwell, C. B. McDanal, and T. J. Matthews.** 1994. Peptides corresponding to a predictive alpha-helical domain of human immunodeficiency virus type 1 gp41 are potent inhibitors of virus infection. Proc. Natl. Acad. Sci. USA 91:9770–9774.
53. **Wiley, D. C., and J. J. Skehel.** 1987. The structure and function of the hemagglutinin membrane glycoprotein of influenza virus. Annu. Rev. Biochem. 56:365–394.
54. **Wilson, I. A., J. J. Skehel, and D. C. Wiley.** 1981. Structure of the haemagglutinin membrane glycoprotein of influenza virus at 3 Å resolution. Nature 289:366–372.
55. **Wintermeyer, S., and M. Nahata.** 1995. Rimantadine: a clinical perspective. Ann. Pharmacother. 29:299–310.
56. **Woods, J. M., R. C. Bethell, J. A. V. Coates, N. Healy, S. A. Hiscox, B. A. Pearson, D. M. Ryan, J. Ticehurst, J. Tilling, S. M. Walcott, and C. R. Penn.** 1993. 4-Guanidino-2,4-dideoxy-2,3-dehydro-*N*-acetylneuraminic acid is a highly effective inhibitor both of the sialidase (neuraminidase) and of growth of a wide range of influenza A and B viruses in vitro. Antimicrob. Agents Chemother. 37:1473–1479.
57. **Xu, X., E. Rocha, H. Regnery, A. Kendal, and N. Cox.** 1993. Genetic and antigenic analyses of influenza A(H1N1) viruses, 1986–1991. Virus Res. 28:37–45.